DNS of soot formation and growth in turbulent non-premixed flames: Damköhler number effects and Lagrangian statistics of soot transport

By A. Attili†, F. Bisetti† AND M. E. Mueller‡

An analysis of soot formation and growth, based on direct numerical simulation of *n*-heptane/air turbulent nonpremixed jet flames, is presented. A detailed chemical mechanism, which includes polycyclic aromatic hydrocarbons, and a high-order method of moments for soot modeling are employed for the first time in a three-dimensional simulation of turbulent sooting flame. It is shown that soot nucleates and grows mainly in the region between 0.3 and 0.5 in mixture fraction space, and it is spread out in the whole mixture fraction space owing to differential diffusion effects. From the analysis of Lagrangian trajectories, it appears that the presence of soot at large values of mixture fraction is related to turbulent fluctuations whose overall effects cannot be captured considering only the average mixing process. Soot moving toward the flame is oxidized, therefore soot mass is negligible for a mixture fraction smaller than 0.25. Finally, it is observed that decreasing by a factor of two the Damköhler number has negligible effects on the overall soot number density while it causes a decrease of a factor of four in the soot volume fraction.

1. Introduction

Soot particles are formed during rich combustion of fossil fuels in technical devices such as internal combustion engines, jet engines, and coal burners (Bockhorn 1994). The carbon mass tied up in particulates is a combustion inefficiency because the full chemical potential of the fuel is not realized via complete conversion of carbon to carbon dioxide. Soot particles are also recognized as an important cause of health complications (Lighty *et al.* 2000; Donaldson *et al.* 2005) such as pulmonary conditions and cancer.

Over the past few years, a few direct numerical simulation (DNS) studies on soot formation in turbulent flames have been performed. Yoo & Im (2007) studied the dynamics of soot formation in turbulent ethylene-air counterflow diffusion flames using DNS. Turbulence increases the global soot yield by increasing flame surface, and it inhibits particle growth by reducing the time soot spends in the high-temperature flame region where growth is most intense.

Narayanan & Trouvé (2009) studied the occurrence of flame weakening, flame extinction, and soot leakage across the flame in a two-dimensional convection-driven turbulent wall-flame configuration using DNS. They concluded that enhanced radiation caused by soot results in frequent flame weakening events and subsequent soot mass leakage across the weakened flame.

Recently, Lignell *et al.* (2007, 2008) performed two DNS studies (2D and 3D) aimed

† Clean Combustion Research Center, King Abdullah University of Science and Technology. Kingdom of Saudi Arabia.
‡ Department of Mechanical and Aerospace Engineering, Princeton University. USA

at examining the effects of soot-flame interaction and soot transport in a temporally evolving jet. The authors highlighted the role of differential diffusion between soot and the gas-phase in determining soot growth rates. They also correlated the direction of transport with soot volume fraction.

Bisetti *et al.* (2012) analyzed the formation and early evolution of soot in a two-dimensional turbulent n-heptane/air flame, using state-of-the-art chemistry and soot models. This study distinguishes itself from previous work (Yoo & Im 2007; Lignell *et al.* 2007, 2008) by considering finite rate chemistry from fuel oxidation to the formation of polycyclic aromatic hydrocarbons (PAH) and a detailed soot model based on elementary physical processes and rates (Blanquart & Pitsch 2009*b*) rather than using a semi-empirical approach (Moss *et al.* 1988; Leung *et al.* 1991).

In the present work, the study by Bisetti *et al.* (2012) is extended to three-dimensional turbulent jets, maintaining the same detailed physical modeling for chemistry and soot. Additional analysis tools are employed, i.e., Lagrangian statistics, and Damköhler number effects are investigated.

A brief description of the physical models and numerical methods is presented in Section 2. Two simulations, characterized by different Damköhler numbers, have been performed and are analyzed in Section 3. The base case (SIM-A) is studied in detail and a preliminary comparison with the second case (SIM-B), characterized by a smaller Damköhler number, is presented.

2. Physical models, numerical methods and configuration description

2.1. *Soot modeling in nonpremixed flames*

Models and methods for the gas phase and soot fields are described in detail in Bisetti *et al.* (2012) and references therein (Mueller *et al.* 2009*b*,*a*; Blanquart & Pitsch 2009*a*) and are reported here briefly.

The gas phase hydrodynamics and combustion are modeled with the reactive, unsteady Navier-Stokes equations in the low Mach number limit (Tomboulides *et al.* 1997). In the present work, the transport of species mass fractions is described with a mixture-averaged diffusion model that takes into account differential diffusion between different species.

Combustion is modeled using a finite rate chemistry approach. The chemical mechanism used is based on the detailed one developed by Blanquart *et al.* (2009) for the high-temperature combustion of engine relevant fuels. A multi-step approach combining automatic and manual reduction techniques has been used to reduce the size of the chemical mechanism and make it more affordable for DNS. The final chemical mechanism obtained at the end of the multi-step reduction procedure contains 47 species and 290 reactions. Complete details on the mechanism reduction and validation can be found in Bisetti *et al.* (2012).

Soot particles and aggregates are described by their volume (V) and surface area (S) (Mueller *et al.* 2009*b*). The bivariate soot moment $M_{x,y}$ (in volume units) is defined as

$$M_{x,y} = \sum_i V_i^x S_i^y N_i, \tag{2.1}$$

where x and y are the moment orders for volume and surface, and V_i, S_i, and N_i are the volume, surface area, and number density of soot aggregates belonging to size class

i. Moments evolve according to the advection-reaction equation:

$$\frac{\partial M_{x,y}}{\partial t} + \frac{\partial (u_i M_{x,y})}{\partial x_i} = \dot{M}_{x,y}, \tag{2.2}$$

where $\dot{M}_{x,y}$ is a source term describing aerosol internal processes. Soot transport is characterized by a high Schmidt number (low diffusivity), and diffusive mass fluxes are therefore neglected. As shown by Bisetti *et al.* (2012), thermophoretic effects (Santoro *et al.* 1987) are also negligible in sooting turbulent nonpremixed jet flames.

The hybrid method of moments (HMOM) closure (Mueller *et al.* 2009*a*) is used with seven statistical moments for the soot population: $M_{0,0}$, $M_{0,1}$, $M_{0,2}$, $M_{1,0}$, $M_{1,1}$, $M_{2,0}$, and N_0. The moment N_0, representing the number of very small particles, is also included in order to describe persistent nucleation in an accurate way. The soot model considers several processes leading to the formation (nucleation), interaction (coagulation), growth (condensation and surface reactions), and destruction (oxidation) of soot particles.

2.2. *Numerical methods*

The gas velocity and reactive scalar fields are solved with a conventional finite-difference scheme (Desjardins *et al.* 2008). The system of advection-reaction equations for soot moments (2.2) is solved with a Lagrangian particle method (Cottet & Koumoutsakos 2000; Koumoutsakos 2005).

The application of a particle method in the context of transport of statistical moments of a distribution has not been analyzed extensively in the literature. Therefore, a brief description of the method is reported here.

It is well known that moment methods coupled with spatial advection encounter numerical difficulties (Wright 2007; Kah *et al.* 2011). The key property of the Lagrangian approach is the independence between advection, described by the movement of particles, and internal processes driven by source terms (nucleation, growth, and coagulation) evolving independently on each particle. Therefore, the Lagrangian scheme is remarkably robust for two reasons: (*a*) errors in the advective fluxes do not pollute the moments set and do not compromise the realizability property of the set and (*b*) the discrete treatment of advection does not involve the computation of gradients, so that stiff source terms do not compromise the stability of the scheme.

In particle methods, functions and differential operators are replaced by equivalent integral representations, discretized using the locations and weights of particles (Koumoutsakos 2005). Particles are mathematical objects representing one or more physical properties, such as temperature, mixture concentration, vorticity, statistical moments of aerosols, etc. The physical properties are evolved by solving a set of ordinary differential equations for the particles' trajectories (x_i^p) and property values (ω^p):

$$\frac{dx_i^p}{dt} = u_i^p = \sum_{q=1}^{N} G(x_i^q, \omega^q, t, ...) \quad \frac{d\omega^p}{dt} = \sum_{q=1}^{N} F(x_i^q, \omega^q, t, ...) \quad p, q = 1, \ldots, N \tag{2.3}$$

where x_i^p and u_i^p denote the location and velocity of particle p, ω^p represents the property vector, and G and F describe the system dynamics. The underlying function represented by the particles at discrete, irregularly spaced points can be approximated as a generalized function (smooth in the sense of the measure) using a sum of delta distributions:

$$\omega(\mathbf{x}, t) = \sum_{p=1}^{N} \omega^p(t) \delta(\mathbf{x} - \mathbf{x}^p(t)), \tag{2.4}$$

Jet centerline initial velocity U_c (m/s)	8.74
Coflow velocity (m/s)	-8.74
Initial jet width H (mm)	15
Jet Reynolds number $Re = \Delta U H/\nu$	15000
Domain size $L_x \times L_y \times L_z$ (mm)	$105 \times 47 \times 23.5$
Simulation time (ms)	30
Grid points $N_x \times N_y \times N_z$	$1024 \times 512 \times 256 \approx 125$ Million
Particles	≈ 300 Million
$\delta x = \delta y = \delta z$ (μm)	91
Kolmogorov scale (minimum) (μm)	110
OH layer thickness (minimum)	$\approx 10\delta x$

TABLE 1. DNS parameters for SIM-A

with $\mathbf{x} = \{x_i\}$. Although the distribution in Eq. (2.4) is well defined, it is desirable to obtain a regular representation (i.e., a differentiable function) of the underlying Eulerian field. Such a representation is obtained via regularization by convolution with a mollification kernel ζ_ε of width ε:

$$\omega(\mathbf{x}, t) \sim (\omega \star \zeta_\varepsilon)(\mathbf{x}, t) = \sum_{p=1}^{N} \omega^p(t) \zeta_\varepsilon(\mathbf{x} - \mathbf{x}^p(t)). \tag{2.5}$$

The Eulerian transport equation for the soot moments (2.2) is solved with the Lagrangian particle approach:

$$\frac{dx_i^p}{dt} = u_i(x_i^p) \quad \text{and} \quad \frac{d\phi^p}{dt} = S^p, \tag{2.6}$$

where $u_i(x_i^p)$ is the Eulerian velocity evaluated at the particle position, ϕ^p represents a vector of soot moments, and S^p is the source term for each particle. The Eulerian fields are reconstructed at the particle positions using a tri-linear interpolation scheme to evaluate the particle velocity $u_i(x_i^p)$ and source term S^p.

If required, the solution obtained with the particle method can be projected via the mollification kernel on a grid that may or may not coincide with the one used for the velocity and scalar fields. The projection of the Lagrangian solution on the grid is needed to post-process the data and to compute source terms for the Eulerian scalars resulting from to soot growth processes, thus enabling a two-way coupling between the aerosol and the gas phase. A box average is used as a regularization kernel:

$$\phi(\mathbf{x}) = \frac{1}{N_\Omega} \sum_{p \in \Omega} \phi^p, \tag{2.7}$$

where Ω is the set of particles located inside a cell of size ε and N_Ω the number of such particles.

2.3. *Temporally evolving jet flame*

The configuration selected for the study is a temporally evolving plane jet. The fuel stream consists of *n*-heptane diluted with 85% (by volume) nitrogen at 400 K. The oxidizer stream consists of air (21% oxygen and 79% nitrogen) at 800 K. In the region of smooth transition between the fuel and oxidizer, a layer, characterized by the equilibrium solution at the stoichiometric composition, has been inserted. This layer mimics the pilot

usually employed in experimental studies of jet flames. The equilibrium solution has been chosen to avoid the presence of soot precursors that would introduce an arbitrary initial soot inception and growth.

The initial condition for the mixture fraction, Z (defined as the field that satisfies an advection-diffusion equation with zero source terms and diffusion equal to that of temperature) is 1 in the fuel core and 0 in the coflow.

For the core of the jet, the initial velocity field is obtained with a simulation of a fully developed turbulent channel at Reynold number $\mathrm{Re}_\tau = 390$. In the coflow region the velocity is obtained mirroring the core average velocity and adding the corresponding fluctuation. Therefore, the velocity difference between the two streams is $\Delta U = 2U_c$.

Periodic boundary condition are applied in the y (streamwise) and z (spanwise) directions. In the x direction (normal to the average flame sheet), open boundary conditions are prescribed in order to allow mass outflow generated by combustion.

Table 1 shows the main physical and numerical parameters for the base configuration (SIM-A). In order to study Damköhler number effects, an additional simulation (SIM-B) has been performed and analyzed. For this second case all thermochemical properties (i.e., composition, initial temperature) and the Reynolds number are the same as SIM-A. The Damköhler number variation is obtained by rescaling the reference size and velocity of the configuration by a factor of $1/\sqrt{2}$ and $\sqrt{2}$, respectively. These changes results in a factor $1/2$ for Damköhler number and a factor of 2 for the scalar dissipation. It has been verified that the variation of scalar dissipation between the two simulations has negligible effects on the density. Therefore, the similarity hypotheses for constant Reynolds number holds, and identical non-dimensional hydrodynamic fields are observed. It can be concluded that the comparison of the results in the two cases allows for the isolation of the effects of different mechanical/chemical time scales ratios on soot and its precursors.

3. Results

3.1. *Analysis of soot fields*

Figure 1 shows naphthalene (one of the PAH molecules and main soot precursor), number density, and volume fraction of soot on a two-dimensional cut of the domain at two different time instants. At 10 ms the center of the jet is not involved yet in the mixing process, and naphthalene and soot are concentrated in a layer close to the flame surface. At later times, naphthalene is present in the entire jet core; the maximum mixture fraction is no longer unity; and soot has been spread out significantly in the region of rich mixture by the turbulent field.

Owing to differential diffusion between the mixture fraction (in general gas phase species) and soot, the latter experiences significant movements in mixture fraction space. Figures 2, 3, and 4 show the number density, volume, and mass fractions of soot in mixture fraction space at several time instants, from the initial phase of the jet development up to the late time solution. Figure 5 displays statistics of the soot mass fraction growth at time $t = 20$ ms. The mass growth for some Lagrangian particles is reported, together with the mean, conditioned on mixture fraction. It is evident that soot grows mainly in the region $0.3 < Z < 0.5$, it is oxidized in the region $0.15 < Z < 0.3$, and source terms approach zero for $Z > 0.6$.

In the first phase of the jet development, soot is concentrated mainly near the flame surface. Up to 1 ms, soot number density grows quickly in the region $0.2 < Z < 0.5$ (Figure 2) in mixture fraction space due to available PAH. Then, coagulation starts to

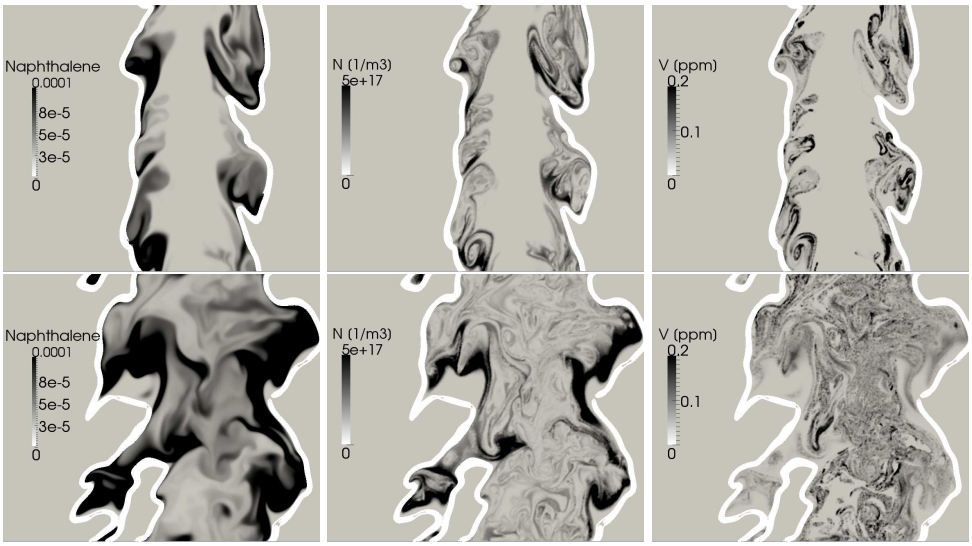

FIGURE 1. Naphthalene (left), soot number density (center), and soot volume fraction (right) at 10 ms (top) and 25 ms (bottom) for SIM-A. The flame is highlighted by the white lines, representing high concentration of HCO.

dominate, and the number density decreases. Meanwhile, turbulent fluctuations, originating from the break-up of the Kelvin-Helmholtz structures and the production by mean shear, induce significant drift of particles in mixture fraction space. At late time, soot is present in the entire fuel-rich side of the mixture fraction space. On the lean side, i.e., $Z < 0.2$, the amount of soot is negligible for the entire duration of the simulation. This is the consequence of two different phenomena: (a) soot, which is generated in the region $0.3 < Z < 0.5$, tends to move preferentially toward reacher mixture. From the analysis of Lagrangian trajectories in mixture fraction space, it is observed that only 6% of the notional particles that experienced some soot growth cross the threshold $Z = 0.2$ and (b) when soot is transported toward leaner mixture, oxidation becomes dominant and consumes all of the soot mass. Oxidation is solely responsible for the negative growth of soot mass that appears in Figure 5. It is likely that only the simultaneous presence of a significant amount of soot moving toward lean mixture fractions, together with some local weakening (extinction) of the flame, could cause non-negligible soot for $Z < 0.2$ (Lignell *et al.* 2008; Narayanan & Trouvé 2009).

Volume and mass fractions of soot grow quickly in time up to 5 ms, reaching a peak value at $Z = 0.4$. From the analysis of Figure 5, it is evident that significant soot formation happens mainly in the region $0.25 < Z < 0.5$. Therefore, the wide range of mixture fractions (in particular for $Z > 0.5$) at which soot is present is due to differential diffusion between soot and mixture fraction and not to soot formation or growth at large mixture fraction values.

Finally, it is interesting to observe that, at later times, the volume fraction profile peaks at very high value of mixture fraction. However, this trend is simply an artifact of the higher density of the gas at these mixture fractions. At the same mixture fractions, the soot mass fraction is smaller than at its maximum near $Z = 0.4$.

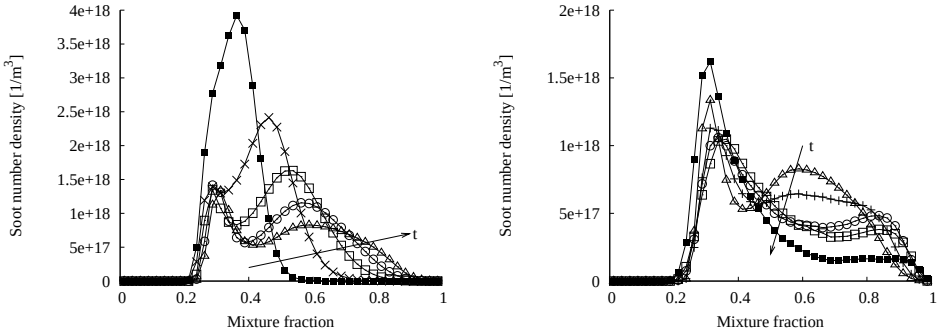

FIGURE 2. Mean number density of soot particulate, conditioned on mixture fraction, at several time instants; results shown for SIM-A. Left figure: number density at 1 ms (filled squares), 2 ms (crosses), 3 ms (open squares), 4 ms (circles), and 5 ms (triangles). Right figure: number density at 5 ms (triangles), 6 ms (plus), 8 ms (circles), 10 ms (open squares), and the late time solution at 25 ms (filled squares). The scale of the number density axes is different in the two figures.

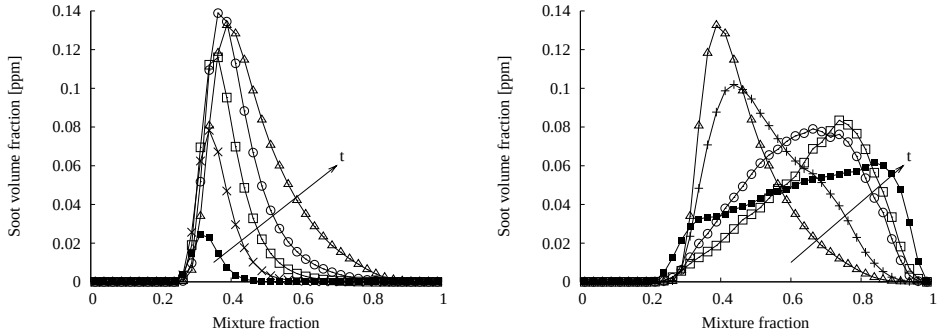

FIGURE 3. Mean volume fraction of soot particulate, conditioned on mixture fraction, at several time instants; results shown for SIM-A. Left figure: volume fraction at 1 ms (filled squares), 2 ms (crosses), 3 ms (open squares), 4 ms (circles), and 5 ms (triangles). Right figure: volume at 5 ms (triangles), 6 ms (plus), 8 ms (circles), 10 ms (open squares), and the late time solution at 25 ms (filled squares).

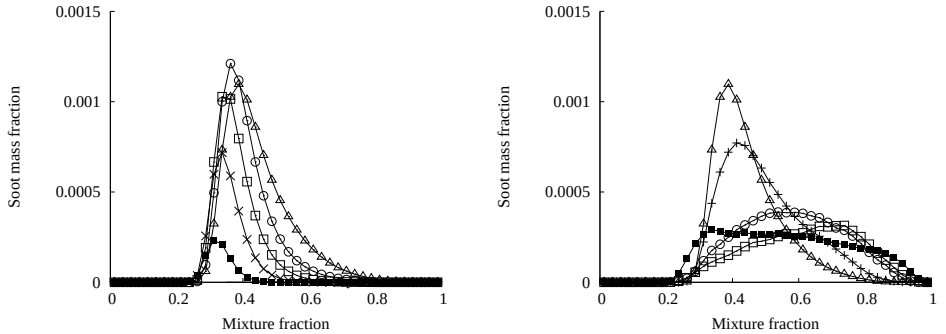

FIGURE 4. Mean mass fraction of soot particulate, conditioned on mixture fraction, at several time instants; results shown for SIM-A. Left figure: mass fraction at 1 ms (filled squares), 2 ms (crosses), 3 ms (open squares), 4 ms (circles), and 5 ms (triangles). Right figure: mass fraction at 5 ms (triangles), 6 ms (plus), 8 ms (circles), 10 ms (open squares), and the late time solution at 25 ms (filled squares).

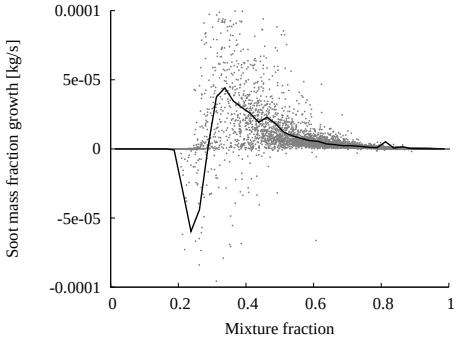

FIGURE 5. Soot mass fraction growth at time $t = 20$ ms; results shown for SIM-A. Every point represents a Lagrangian particle and the time derivative is computed on the Lagrangian trajectory. Only a small fraction of the entire set of particles is shown. Mean soot mass fraction growth conditioned on mixture fraction (line).

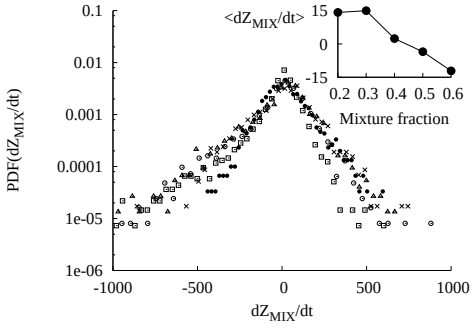

FIGURE 6. PDFs of Lagrangian time derivative of mixture fraction conditioned on several value of mixture fraction at time $t = 20$ ms; results shown for SIM-A. $Z = 0.2$ (filled circles), 0.3 (crosses),0.4 (open triangles), 0.5 (open circles), 0.6 (open squares). Inset: mean value for the distributions shown in the main figure.

3.2. *Lagrangian statistics*

Given the fundamental importance of soot movement in mixture fraction space (and more generally composition space), further statistical analysis of this process is performed. Lagrangian statistics are the most appropriate tool to study the evolution of soot during its movement in physical and mixture fraction space.

Figure 6 shows probability density functions of the Lagrangian time derivative of mixture fraction conditioned on several values of the mixture fraction itself. The inset displays the mean of these distributions. This time derivative characterizes the movement of soot in mixture fraction space and can be considered analogous to the displacement velocity used in previous works (Lignell *et al.* 2008; Bisetti *et al.* 2012). The mean is positive for mixture fraction $Z < 0.4$ whereas it is negative for $Z > 0.4$. Positive values correspond to a mean tendency of Lagrangian particles to move toward rich mixtures. The PDFs shows large exponential tails with values much larger than the root mean square (not shown), a signature of the intermittent nature of the turbulent field. These large fluctuations are responsible for soot drift in mixture fraction space. In particular, it is interesting to observe that large amounts of soot appears at very high mixture fractions $Z > 0.7$ (Figure 4), even if the mean Lagrangian derivative is negative for $Z > 0.4$. Therefore, the transport of soot to regions with very high mixture fraction is related to turbulent fluctuations whose overall effects cannot be captured considering only the mean mixing process. The Lagrangian analysis presented refers to a single instant. Nevertheless, a similar behavior has also been observed at different time instants. Finally, realistic three-dimensional turbulence has to be considered in order to correctly characterize soot evolution, due to the important role of large fluctuations and small scale intermittency that do not appear in two-dimensional turbulence (Bernard *et al.* 2006).

3.3. *Damköhler number effects*

The effects of Damköhler number variations on the overall soot amount is reported in Figure 7. The total volume of soot for the large Damköhler number case (i.e., smaller scalar dissipation) is approximately four times larger than the value observed in the

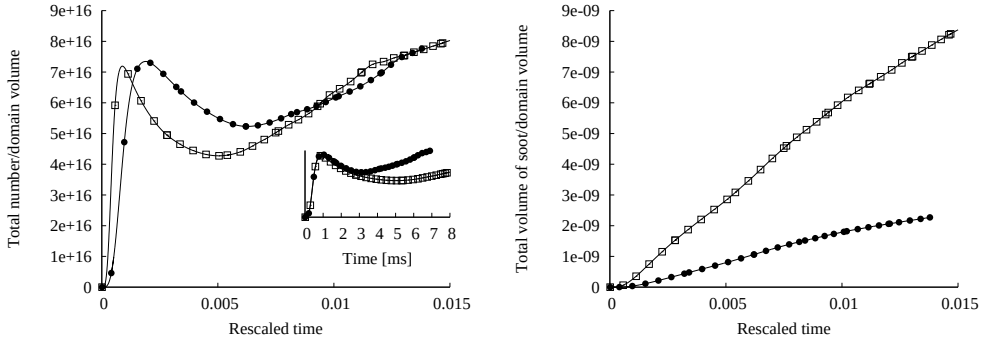

FIGURE 7. Time evolution of total (integrated over the entire domain) number density (left) and volume fraction (right) of soot, rescaled with the domain volume. The results for the two case with different Damköhler number effects are shown: large Damköhler, SIM-A (open symbols) and small Damköhler, SIM-B (filled symbols). The time axes of the two graphs are rescaled with the hydrodynamic timescale. Inset in left graph: number density for the two simulations versus physical time in the first phase of the jet evolution.

small Damköhler number case. At late times, the total number densities in the two cases show a similar growth rate if plotted versus a time axis rescaled with the hydrodynamic timescale. It is worth noting that the hydrodynamic timescale for the large Damköhler number case is two times that for the small Damköhler number configuration. During the first phase the total number density increases quickly and, as coagulation becomes dominant, reaches the same peak value for the two cases. It is interesting to note that, if the time is not rescaled (i.e., the physical time is used, see inset in Figure 7), the value of the total number density is nearly identical for the two cases up to 3 ms. This behavior can be explained by the fact that, in the first phase of the jet development, soot evolution is governed by the nucleation and coagulation timescale, that is the same for the two cases, with negligible effects of scalar dissipation rate.

Acknowledgments

We acknowledge valuable support from KAUST Supercomputing Laboratory in the form of assistance with code development and computational time on the IBM System Blue Gene/P "Shaheen" at King Abdullah University of Science and Technology.

REFERENCES

BERNARD, D., BOFFETTA, G., CELANI, A. & FALKOVICH, G. 2006 Conformal invariance in two-dimensional turbulence. *Nature Physics* **2** (2), 124–128.

BISETTI, F., BLANQUART, G., MUELLER, M. & PITSCH, H. 2012 On the formation and early evolution of soot in turbulent nonpremixed flames. *Combust. Flame* **159** (1), 317–335.

BLANQUART, G., PEPIOT-DESJARDINS, P. & PITSCH, H. 2009 Chemical mechanism for high temperature combustion of engine relevant fuels with emphasis on soot precursors. *Combust. Flame* **156** (3), 588–607.

BLANQUART, G. & PITSCH, H. 2009*a* Combustion generated fine carbonaceous particles. *in: H. Bockhorn, A. D'Anna, A.F. Sarofim and H. Wang, (Eds), Combustion Generated Fine Carbonaceous Particles* pp. 437–463.

BLANQUART, G. & PITSCH, H. 2009*b* A joint Volume-Surface-Hydrogen multi-variate

model for soot formation. In *Combustion Generated Fine Carbonaceous Particles* (ed. H. Bockhorn, A. D'Anna, A. F. Sarofim & H. Wang), pp. 437–463. KIT Scientific Publishing.

Bockhorn, H. 1994 *Soot formation in combustion*. New York: Springer-Verlag.

Cottet, G. & Koumoutsakos, P. 2000 *Vortex methods: theory and practice*. Cambridge Univ Press.

Desjardins, O., Blanquart, G., Balarac, G. & Pitsch, H. 2008 High order conservative finite difference scheme for variable density low mach number turbulent flows. *J. Comput. Phys.* **227**, 7125–7159.

Donaldson, K., Tran, L., Jimenez, L. A., Duffin, R., Newby, D. E., Mills, N., MacNee, W. & Stone, V. 2005 Combustion-derived nanoparticles: A review of their toxicology following inhalation exposure. *Part. Fibre Toxicol.* **2** (10), 1–14.

Kah, D., Laurent, F., Massot, M. & Jay, S. 2011 A high order moment method simulating evaporation and advection of a polydisperse liquid spray. *J. Comput. Phys.* **231** (2), 394–422.

Koumoutsakos, P. 2005 Multiscale flow simulations using particles. *Annu. Rev. Fluid Mech.* **37**, 457–487.

Leung, K. M., Lindstedt, R. P. & Jones, W. P. 1991 A simplified reaction mechanism for soot formation in nonpremixed flames. *Combust. Flame* **87**, 289–305.

Lighty, J. S., Veranth, J. M. & Sarofim, A. F. 2000 Combustion aerosols: Factors governing their size and composition and implications to human health. *J. Air Waste Manage. Assoc.* **50**, 1565–1618.

Lignell, D. O., Chen, J. H. & Smith, P. J. 2008 Three-dimensional direct numerical simulation of soot formation and transport in a temporally evolving nonpremixed ethylene jet flame. *Combust. Flame* **155**, 316–333.

Lignell, D. O., Chen, J. H., Smith, P. J., Lu, T. & Law, C. K. 2007 The effect of flame structure on soot formation and transport in turbulent nonpremixed flames using direct numerical simulation. *Combust. Flame* **151**, 2–28.

Moss, J. B., Stewart, C. D. & Syed, K. J. 1988 Flowfield modelling of soot formation at elevated pressure. *Proc. Combust. Inst.* **22**, 413–423.

Mueller, M., Blanquart, G. & Pitsch, H. 2009*a* Hybrid method of moments for modeling soot formation and growth. *Combust. Flame* **156** (6), 1143–1155.

Mueller, M., Blanquart, G. & Pitsch, H. 2009*b* A joint volume-surface model of soot aggregation with the method of moments. *Proc. Combust. Inst.* **32** (1), 785–792.

Narayanan, P. & Trouvé, A. 2009 Radiation-driven flame weakening effects in sooting turbulent diffusion flames. *Proc. Combust. Inst.* **32**, 1481–1489.

Santoro, R. J., Yeh, T. T., Horvath, J. J. & Semerjian, H. G. 1987 The transport and growth of soot particles in laminar diffusion flames. *Combust. Sci. Technol.* **53**, 89–115.

Tomboulides, A., Lee, J. & Orszag, S. 1997 Numerical simulation of low mach number reactive flows. *J. Sci. Comput.* **12** (2), 139–167.

Wright, D. 2007 Numerical advection of moments of the particle size distribution in eulerian models. *J. Aerosol Sci.* **38** (3), 352–369.

Yoo, C. S. & Im, H. G. 2007 Transient soot dynamics in turbulent nonpremixed ethyleneair counterflow flames. *Proc. Combust. Inst.* **31**, 701–708.